

Twin-S: A Digital Twin Paradigm for Skull Base Surgery

Hongchao Shu^{1*†}, Ruixing Liang^{1,2†}, Zhaoshuo Li^{1†}, Anna Goodridge¹, Xiangyu Zhang¹, Hao Ding¹, Nimesh Nagururu², Manish Sahu¹, Francis X. Creighton², Russell H. Taylor¹, Adnan Munawar¹ and Mathias Unberath¹

¹Johns Hopkins University, Baltimore, MD, United States.

²Johns Hopkins Medicine, Baltimore, MD, United States.

*Corresponding author(s). E-mail(s): hshu4@jhu.edu;

†These authors are joint first authors.

Abstract

Purpose: Digital twins are virtual replicas of real-world objects and processes. This paradigm has great potential in surgical procedures, for example by enhancing the situational awareness of surgeons. We introduce *Twin-S*, a digital twin framework for skull base surgery. **Methods:** *Twin-S* combines high-precision optical tracking and real-time simulation. To guarantee accurate modeling, *Twin-S* is enabled by calibration routines to ensure that the virtual representation precisely reflects all real-world processes. *Twin-S* models and tracks key elements of skull base surgery, including surgical tools, patient anatomy, and surgical cameras. Importantly, *Twin-S* models real-world drilling and updates the virtual model at a frame rate of 28. **Results:** Our evaluation of *Twin-S* demonstrates an average error of 1.39 mm during the drilling process. Our study also highlights the benefits of *Twin-S* in downstream applications in image-guided interventions. We showcase how *Twin-S* provides temporally varying augmented overlays derived from the continuously updated virtual model, thus offering additional situational awareness to the surgeon. **Conclusion:** Our digital twin paradigm captures the real-world surgical progress and updates the virtual model in real-time through modern tracking technologies. Future research integrating vision-based techniques could further increase the accuracy of *Twin-S*.

Keywords: Image-guided Intervention; Human-computer Interaction; Intervention Planning and Simulation; Surgical Data for Machine Learning;

1 Introduction

Digital twins are virtual counterparts of real-world processes, modeling dynamics and properties in real-time [1]. Receiving continuous measurements from sensor-rich environments, digital twins can conversely provide computational feedback, which is difficult to obtain otherwise. Digital twins have been widely adopted in areas of manufacturing, farming, and product design [2]. In biomedical sciences, digital twins are used in cardiovascular diagnostics [3], insulin pump control [4], and etc. Digital twins are also envisioned to aid personalized medication [5] and predict human immune system responses [6].

In surgical scenarios, digital twins can potentially offer advantages across all surgical stages (Figure 1). Prior work has explored the use of digital twins in pre-operative planning and surgical training [7]. When used intra-operatively, digital twins can provide real-time guidance to surgeons for complementary situational awareness and, in turn, facilitate surgical decision-making [8–10]. Lastly, digital twins can fully digitize the procedures for record-keeping, post-operative evaluation, and dataset generation for machine learning algorithms.

Some of the earliest works related to the concept of digital twins for surgical assistance date back to 1994. RobotDoc [11, 12], a robotic system for orthopedic surgeries, visualized CT pre-operative scans and highlighted drilled tissues for guidance. Subsequently, many solutions have been presented with more advanced model updating techniques and visualizations. For example, Chalasani *et. al.* [13] and Yasin *et. al.* [14] update the pre-operatively acquired organ model based on force sensing while surgeons palpate the tissue. Concurrent to our work, Shi *et al.* [15] uses a digital twin paradigm in liver tumor surgery, where a virtual model is used to predict the motion of the liver for respiratory compensation. Digital twin frameworks also have found applications in telesurgery [16, 17].

Augmented Reality (AR) and Virtual Reality (VR) also closely relate to digital twin systems and have been widely adopted for surgical applications [18]. Most prior AR systems overlay the pre-operative scans or plans on the patient anatomy for intra-operative guidance [19]. However, these systems do not update the patient model intra-operatively, limiting their applications [20]. VR systems, on the other hand, mainly focus on simulations for surgical training [21]. These VR systems do not receive measurements from the real world, and thus fail to mimic the behaviors of the physical entities in real-time [22, 23].

We present a digital twin framework named Twin-S for skull base surgeries. We specifically consider mastoidectomy [24], a surgical approach in the lateral skull base whereby bone is removed with surgical drills to obtain access to the middle and inner ear. Given the complex arrangement of cortical bone,

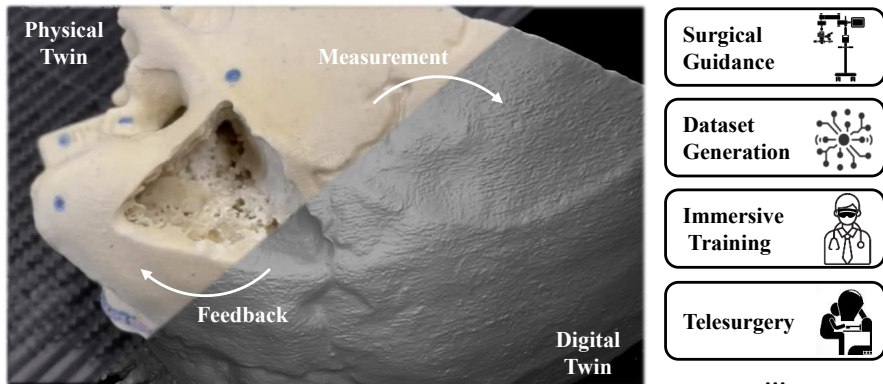


Fig. 1 In our Twin-S paradigm, measurements are collected from sensors deployed in the operating room and sent to the digital twin continuously. The computation analysis of the simulation feedback to the physical twin. The proposed digital twin setup enables many downstream applications across various surgical stages.

nerves, vasculature, and end-organs, surgical stereo microscopes are used to navigate in the small operating field. Twin-S combines high-precision optical tracking and real-time physics-based simulation [22, 23]. We rely on calibration routines to ensure that the virtual representation precisely mimics all real-world processes. Twin-S models and tracks the critical components of skull base surgery, including the surgical tool, patient anatomy, and surgical camera. Twin-S updates the virtual patient anatomy model to account for the real-world tool-to-tissue interactions at a frame rate of 28 FPS.

We conduct experiments to evaluate the accuracy of each component of Twin-S. We further derive numerical analysis to provide maximum bounds on tracking error and the contribution to the final error from different stages. Finally, we illustrate one use case of Twin-S to improve situational awareness in a mixed-reality setup. The contributions can be summarized as follows:

- We present a digital twin framework for skull base surgery named Twin-S. It models, tracks and updates all critical components of skull base surgeries in real-time to mimic real-world processes.
- We conduct evaluations on tracking accuracy and simulation fidelity of Twin-S. We present numerical analysis for the worst-case error bounds.
- We showcase one application of Twin-S in downstream mixed reality tasks to provide surgical guidance and context situational awareness.

2 System Components

Building a digital twin system for skull base surgery requires precise modeling, tracking, and updating of the patient’s anatomy, the surgeon’s tool(s), and the surgical camera. In our setup, the system includes a surgical phantom to simulate the patient’s anatomy, a surgical drill as the ablation tool, and a stereo surgical microscope. Twin-S acquires 3D poses of each component via

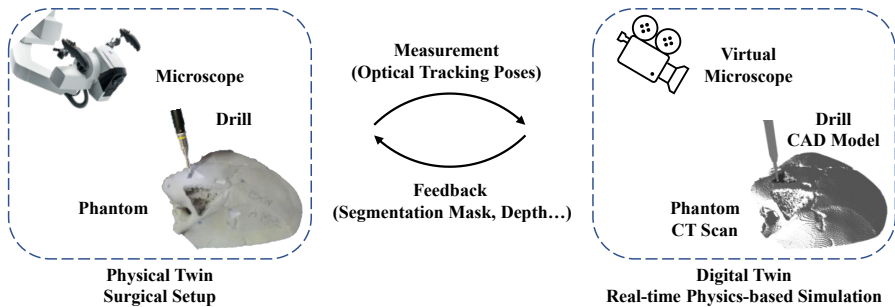


Fig. 2 Twin-S models, tracks, and updates the surgical drill, phantom, and microscope to emulate the skull base surgical setting. Optical tracking provides measurements of object poses to the digital twin. Using the CT scan of the phantom and the drill model, a real-time physics-based simulation replicates the real-world processes. The simulation generates computational feedback such as segmentation mask and depth back to the physical twin.

an optical tracker (FusionTrack 500, Atracsys¹). We use o to denote the optical tracker. The pose measurements are streamed into a physics-based real-time simulation built upon AMBF [22, 23]. The simulation provides computational analysis as feedback to real-world processes. An overview is shown in Figure 2.

2.1 Modeling of the Surgical Drill

The 3D model of the surgical tool is obtained from its manufacturer (ANSPACH, Johnson & Johnson²). In Twin-S, we define the drill coordinate frame to be the drill tip center. We mount the optical tracking markers at the drill shaft’s tail, defining the drill’s base coordinate. We need to calibrate the transformation from the *drill’s* base coordinate to the *drill* coordinate ${}^{db}F_d$.

The translational component ${}^{db}t_d$ is obtained by pivot calibration [25]. For the rotational component ${}^{db}R_d$, it is only necessary to calibrate two degrees of freedom as the drill is symmetrical along its shaft. The calibration reduces to aligning two directions – the shaft direction in the drill coordinate (denoted as \vec{P}) and in the optical tracker coordinate (denoted as \vec{Q}). Using the Kabsch algorithm [26], the rotation can be recovered as:

$${}^{db}R_d = (H^T H)^{\frac{1}{2}} H^{-1}, \text{ where } H = \vec{P}^T \vec{Q}. \quad (1)$$

The shaft direction in the drill coordinate \vec{P} is defined to be along the Z-axis and thus is known. To recover the shaft direction in optical tracker coordinate \vec{Q} , we fix the drill on a robot arm end effector, where the drill holder by design aligns the drill shaft with the Z-axis of the robot to sufficient accuracy [27]. Therefore, by commanding the robot to move along its Z-axis, we recover the direction of motion \vec{Q} in the optical tracker coordinate. Given known \vec{P} and measured \vec{Q} , we can recover ${}^{db}R_d$ up to two degrees of freedom.

¹<https://www.atracsys-measurement.com/products/fusiontrack-500/>

²<https://www.jnjmedtech.com/en-EMEA/product/anspach-eg1-electric-system>

2.2 Modeling of the Surgical Phantom

We obtain the 3D structure of the surgical phantom using a CT scanner (Loop-X, Brainlab³). The phantom is modeled as a binary volume of occupancy, where voxels corresponding to the bony tissues are marked as occupied and voxels representing air are marked as free space. To track the surgical phantom, we rigidly mount the phantom on a polycarbonate board with optical tracking markers, defining the base coordinate of the phantom. To calibrate the transformation from *phantom base* to *phantom* ${}^{pb}F_p$, we directly compute the transformation between the virtual model and the physical phantom via the point-to-plane ICP registration [28]. We sample 380 points on the physical phantom surface using a tracked pointer tool for the purpose of calibration.

2.3 Modeling Tool-to-tissue Interaction

When surgeons perform drilling in the real world, we update the surgical phantom in real-time. We approximate the drill tip as a sphere and detect collisions between the surgical phantom and the drill tip given the tracked positions. The voxels that collide with the drill tip are moved and set to free space to simulate the tissue removal process. More details of the drilling algorithm can be found in prior work [22].

2.4 Modeling of the Surgical Camera

We obtain the intrinsic parameters and distortion coefficients of the stereo camera using a ChArUco pattern. Rectification is then performed to obtain a projective camera model [29]. To track the surgical camera, optical tracking markers are mounted on the handle of the camera, defining the base coordinate frame. A hand-eye calibration routine [30, 31] is used to obtain the transformation from the camera *base* coordinate to the *camera* coordinate ${}^{cb}F_c$. Given the tracked camera, Twin-S generates per-pixel segmentation mask and depth maps based on the object information [22], which can be used for different downstream applications.

3 Experiments and Results

In the following sections, we conduct experiments and numerical analysis on Twin-S to characterize its accuracy.

3.1 Optical Tracking Accuracy

We conduct experiments to evaluate the accuracy of the optical tracker, as its accuracy directly impacts the results of Twin-S. Throughout the experiment, we put the optical tracker at a fixed location. We mount the optical markers on a 3-axis micrometer stage (Figure 3 (a)). For each experiment trial, we individually move 5 mm along the x, y, and z axis in the micrometer stage

³<https://www.brainlab.com/loop-x>

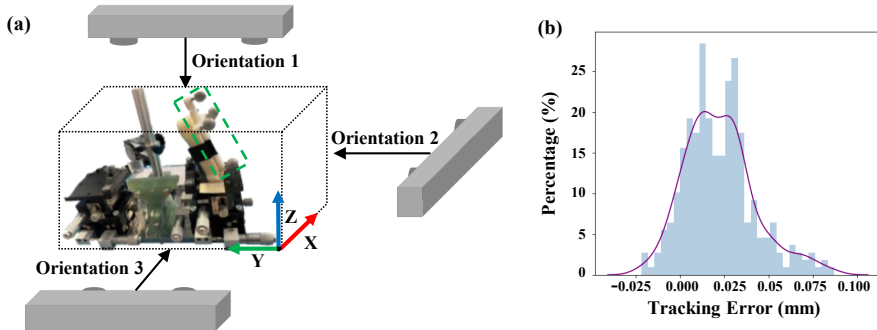


Fig. 3 (a) Optical tracker evaluation setup, 4 optical tracking markers are fixed on a 3-axis micrometer stage. Relative orientations of the micrometer stage w.r.t the optical tracker. (c) Histogram of tracking errors.

local coordinate. We conduct 3 trials in total, each with a new orientation w.r.t. the optical tracker (Figure 3 (a)). The histogram of error is plotted in Figure 3 (b). The mean error is 0.02 mm, with a standard deviation of 0.02 mm and a maximum error of 0.08 mm. We find the sub-millimeter accuracy of the optical tracker sufficient for our purpose. We provide additional evaluation results along each axis and the impact of rotation in Appendix A.

3.2 Camera Calibration Accuracy

We assess the accuracy of camera calibration as it is critical to downstream applications such as mixed reality and machine learning data generation. To perform a quantitative evaluation of hand-eye calibration, we move the camera to different locations observing a static ChArUco pattern. The image resolution is 1920×1080 . We take the first video frame as the reference frame. The reference frame is then transformed and projected into subsequent video frames. We evaluate the alignment of the projected pattern and observed pattern and report the re-projection error (RPE) among all frames.

The hand-eye calibration method only has a 16 pixels mean RPE, which is equivalent to 0.8% of the image width. We further convert the pixel RPE to calibration errors in mm by exploiting the projective relationship between the image space and the Cartesian coordinate using the following equation:

$${}^c\epsilon_u/\text{RPE} = {}^c t_u/f_{px}. \quad (2)$$

In other words, the ratio between the calibration error ${}^c\epsilon_u$ in mm and mean RPE in pixels is equal to the ratio between the camera-to-ChArUco distance ${}^c t_u$ in mm and surgical camera focal length f_{px} in pixels. Given the estimate of ${}^c t_u$ from the physical setup and the calibrated camera focal length f_{px} , the hand-eye calibration error converts approximately to 1.9 mm.

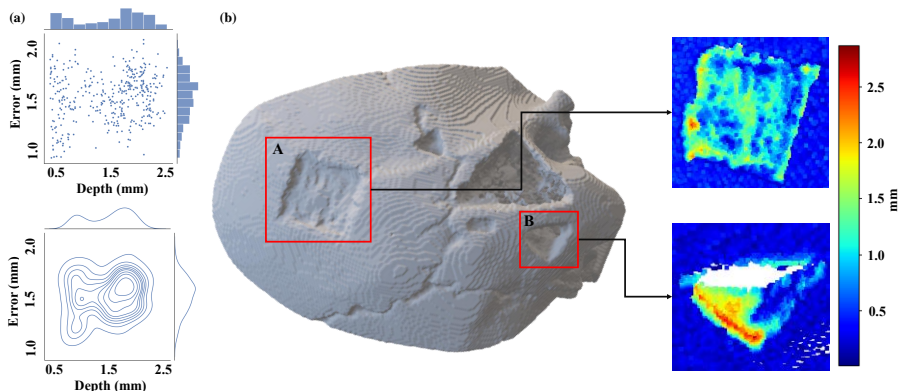


Fig. 4 (a) Scatter and density plots of drilling depth and simulation error. We have not found a statistically significant correlation between drilling depth and error (p -value=1). (b) Evaluation of misalignment between ground truth CT scan and a phantom point cloud from the virtual model. The lower error indicates better agreement between the CT scan and the virtually updated model from Twin-S.

3.3 Drilling Simulation Accuracy

One of the key features of Twin-S is the real-time updating of the anatomic model as the patient’s anatomy is ablated. We experiment to evaluate the accuracy of the drilling process. A surgical expert is invited to drill the surgical phantom similar to *in vivo* mastoidectomy. We compare the updated phantom model of our Twin-S framework after drilling with the 3D structure obtained by a Loop-X CT scanner. We visualize the mismatch between the virtual estimate of the tissue ablation and the true state of the phantom after the surgery as a heat map in Figure 4 (b). We report the error in drilled regions only instead of the entire model to evaluate the model update accuracy of Twin-S.

The mean error of our virtual model in region A is 1.18 mm with a standard deviation of 0.24 mm, and the mean error in region B is 1.61 mm with the standard deviation of 0.49 mm. The average error of all drilled regions is 1.39 mm with a standard deviation of 0.62 mm. Errors are mostly located around sharp edges, which are affected to some extent by the limited spatial resolution of the CT scan. We further examine if there is correlation between the drilling depth and error, with qualitative results shown in Figure 4 (a). We do not observe strong correlations between the two variables qualitatively, and the p -value of 1 from our chi-square test confirms that the variables are indeed statistically independent.

Overall, the results indicate that Twin-S can update the anatomical model with a precision comparable to conventional optical navigation systems [32], which is expected since spatial tracking in Twin-S largely relies on those systems. However, the average drilling depth of 1.57 mm is shallower than clinical practices [33]. The line-of-sight issues of the optical tracking system currently prohibit us from drilling deeper. It is our future work to resolve the line-of-sight issue and expand our evaluation in deeper regions.

3.4 Numerically Analyzing Tracking Performance

We analyze the tracking error to shed insights into sources of error in the tracking performance. We denote the measured transformation as F^* , which contains error ΔF and deviates from the actual transformation F :

$$F^* = F \cdot \Delta F, \text{ where } \Delta F = \begin{bmatrix} I + \vec{\alpha}^\wedge, & \vec{\varepsilon} \\ 0, & 1 \end{bmatrix}. \quad (3)$$

The α is the rotational error using axis-angle notation, and $(\cdot)^\wedge$ is a skew-symmetric matrix given a vector input. The $\vec{\varepsilon}$ is the translation error.

We present an analysis of the relative pose error between phantom and drill, which is critical for modeling tool-to-tissue interactions. The measured phantom-to-drill transformation is expressed as:

$$\begin{aligned} {}^dF_p^* &= {}^oF_d^{*-1} \cdot {}^oF_p^*, \\ &= ({}^oF_{db}^* \cdot {}^{db}F_d^*)^{-1} \cdot {}^oF_{pb}^* \cdot {}^{pb}F_p^*. \end{aligned} \quad (4)$$

In the following content, we use the rotational component as an example to illustrate our derivation and analysis. We expand the error terms of the rotation part and obtain:

$$\begin{aligned} {}^dR_p^* &= {}^{db}R_d^{*-1} \cdot {}^oR_{db}^{*-1} \cdot {}^oR_{pb}^* \cdot {}^{pb}R_p^*, \\ {}^dR_p \cdot (I + {}^d\vec{\alpha}_p^\wedge) &= \left({}^{db}R_d \cdot (I + {}^{db}\vec{\alpha}_d^\wedge) \right)^{-1} \cdot \left({}^oR_{db} \cdot (I + {}^o\vec{\alpha}_{db}^\wedge) \right)^{-1} \\ &\quad \cdot {}^oR_{pb} \cdot (I + {}^o\vec{\alpha}_{pb}^\wedge) \cdot {}^{pb}R_p \cdot (I + {}^{pb}\vec{\alpha}_p^\wedge). \end{aligned} \quad (5)$$

With re-arrangement, we can obtain 4 independent components contributing to the rotational error:

$${}^d\vec{\alpha}_p = \beta_1 \cdot {}^{pb}\vec{\alpha}_p + \beta_2 \cdot {}^o\vec{\alpha}_{pb} + \beta_3 \cdot {}^o\vec{\alpha}_{db} + \beta_4 \cdot {}^{db}\vec{\alpha}_d, \quad (6)$$

where $\beta_1 = I$, $\beta_2 = {}^{pb}R_p^{-1}$, $\beta_3 = -{}^{pb}R_p^{-1} \cdot {}^oR_{pb}^{-1} \cdot {}^oR_{db}$, and $\beta_4 = -{}^dR_p^{-1}$. Intuitively, the norm of β_i represents how much each measurement error contributes to the final inaccuracy.

To derive the numerical upper bound on tracking error, we use the worst-case tracking accuracy of 0.08 mm for each optical marker obtained from [Sect. 3.1](#). We also assume a worst-case rotation error of 0.5° for ICP as it is not directly obtainable. We obtain the estimated worst-case error norm as:

$$\begin{aligned} \left\| {}^d\vec{\alpha}_p \right\|_2 &\leq \|\beta_1 \cdot {}^{pb}\vec{\alpha}_p\|_2 + \|\beta_2 \cdot {}^o\vec{\alpha}_{pb}\|_2 + \|\beta_3 \cdot {}^o\vec{\alpha}_{db}\|_2 + \|\beta_4 \cdot {}^{db}\vec{\alpha}_d\|_2, \\ &\leq 0.5 + 0.3 + 0.4 + 0.5 = 1.7^\circ. \end{aligned} \quad (7)$$

Table 1 Computation evaluation of Twin-S

Processes of Twin-S	Mean Computational Time (ms)
Data synchronization	20.5
Pose update	0.2
Simulator volume rendering	12.0
Collision simulation	3.0
Overall	35.7

The rotational error $d_{\alpha_p}^{\vec{}}$ is up to 2.7° and dominated by $pb_{\alpha_p}^{\vec{}}$ and $db_{\alpha_d}^{\vec{}}$, which are the calibration inaccuracies. A similar analysis can be done on the translation error $d_{\varepsilon_p}^{\vec{}}$, with the worst error bound of 5.29 mm.

The estimated numerical upper bounds of the tracking error represent the worst-case scenario that Twin-S may produce. In practice, we observe the actual drilling error of 1.39 mm (Sect. 3.3) is much smaller than the estimated upper bounds. Details of the translation error analysis are in Appendix B.

3.5 Segmentation Mask Evaluation

As mentioned in Sect. 2.4, Twin-S can generate per-pixel segmentation masks from the virtual models for downstream applications. Therefore, we evaluate the accuracy of virtually generated segmentation masks and report the Dice scores, where higher Dice scores indicate better accuracy [34]. To obtain ground truth, we manually label a sequence of 100 frames. The Dice score for the drill is 0.725, and the Dice score for the phantom is 0.956. The lower Dice score of the drill in comparison to the phantom is due to the thin shape of the drill, where slight offsets will lead to much lower Dice scores.

3.6 Runtime Performance Evaluation

We conduct a computation evaluation of Twin-S on a laptop of Ubuntu 20.04 equipped with Nvidia 3060 Laptop Graphic card and Intel i5 CPU. The breakdown of the computation time is presented in Table 1. The data synchronization step is the most time-consuming process of 20.5 ms, which aligns the timestamps and pairs the incoming tracking poses from the optical tracker and stereo images from the surgical camera. The overall run time of Twin-S is 35.7 ms (28 FPS).

The calibration step is a requirement prior to launching Twin-S such that the virtual models are aligned with the physical objects. Therefore, the calibration process does not impact the runtime performance of Twin-S. The time spent for calibration is approximately 10 minutes.

4 Use Case in Mixed Reality

We explore a mixed reality use case for providing complementary situational awareness using contextually updated virtual content. We consider the scenario where a pre-operative plan is available for the desired bone ablation in the temporal bone. We present a temporally adaptive overlay to encode the distance

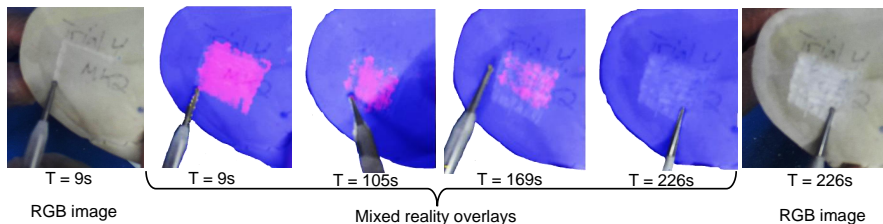


Fig. 5 An illustration of using Twin-S for mixed reality intra-operative guidance. The color overlays generated from the virtual model encode the distance to the deep-seated target.

between the current drilled surface and the deeper-seated target. In doing so, we offer depth information that may be difficult for surgeons to observe due to bone dust, blood, and etc. To demonstrate this idea with Twin-S, we reverse the drilling process and use the final drilled shape as the “pre-planned target” to mimic the targeted application and display the drilling status in previous video frames. Specifically, Twin-S displays a warmer color when the surface is far from the target, and a cooler color as the revealed anatomy is closer to the target. Qualitative visualizations are shown in Figure 5. Such an experiment conceptually demonstrates how Twin-S can be applied to intra-operative guidance, albeit the simple human-computer interaction paradigm. It is our future work to build a fully functional mixed-reality system with more effective graphics interfaces.

5 Conclusion

We present Twin-S, a digital twin framework for skull base surgery. Twin-S models, tracks, and updates virtual counterparts of physical entities in real-time with high accuracy. We present a thorough analysis of the tracking performance and illustrate how Twin-S can be used for downstream applications.

In future work, we plan to integrate vision-based tracking algorithms [35] to further improve the accuracy of Twin-S rather than relying solely on optical trackers. Moreover, Twin-S can generate large-volume of paired data, where microscopic images of the surgical scene are paired with virtually generated labels. Through this pairing, we are able to reduce the cost of dataset labeling and avoid the sim-to-real transfer issue commonly faced by synthetic data [36, 37]. It is our future work to demonstrate the application of Twin-S in dataset generation. Lastly, Twin-S enables model-based control [38] applications of varying anatomies, thus improving surgical safety and patient outcomes.

Acknowledgments. This work was supported in part by Johns Hopkins University internal funds, an agreement between Johns Hopkins University and the Multi-Scale Medical Robotics Centre Ltd., and in part by NIDCD K08 Grant DC019708.

Declarations

Conflict of interest. Russell H. Taylor and Johns Hopkins University (JHU) may be entitled to royalty payments related to technology discussed in this paper, and Dr. Taylor has received or may receive some portion of these royalties. Also, Dr. Taylor is a paid consultant to and owns equity in Galen Robotics, Inc. These arrangements have been reviewed and approved by JHU in accordance with its conflict of interest policy.

References

- [1] Inc., I.: What is a digital twin? | IBM. <https://www.ibm.com/topics/what-is-a-digital-twin> Accessed 2022-8-13
- [2] Jones, D., Snider, C., Nassehi, A., Yon, J., Hicks, B.: Characterising the digital twin: A systematic literature review. *CIRP Journal of Manufacturing Science and Technology* **29**, 36–52 (2020)
- [3] Martinez-Velazquez, R., Gamez, R., El Saddik, A.: Cardio twin: A digital twin of the human heart running on the edge. In: 2019 IEEE International Symposium on Medical Measurements and Applications (MeMeA), pp. 1–6 (2019). IEEE
- [4] Breton, M.D., Kanapka, L.G., Beck, R.W., Ekhlaspour, L., Forlenza, G.P., Cengiz, E., Schoelwer, M., Ruedy, K.J., Jost, E., Carria, L., *et al.*: A randomized trial of closed-loop control in children with type 1 diabetes. *New England Journal of Medicine* **383**(9), 836–845 (2020)
- [5] Björnsson, B., Borrebaeck, C., Elander, N., Gasslander, T., Gawel, D.R., Gustafsson, M., Jörnsten, R., Lee, E.J., Li, X., Lilja, S., *et al.*: Digital twins to personalize medicine. *Genome medicine* **12**, 1–4 (2020)
- [6] Laubenbacher, R., Niarakis, A., Helikar, T., An, G., Shapiro, B., Malik-Sheriff, R., Segó, T., Knapp, A., Macklin, P., Glazier, J.: Building digital twins of the human immune system: toward a roadmap. *npj Digital Medicine* **5**(1), 64 (2022)
- [7] Coelho, G., Rabelo, N.N., Vieira, E., Mendes, K., Zagatto, G., de Oliveira, R.S., Raposo-Amaral, C.E., Yoshida, M., de Souza, M.R., Fagundes, C.F., *et al.*: Augmented reality and physical hybrid model simulation for preoperative planning of metopic craniosynostosis surgery. *Neurosurgical focus* **48**(3), 19 (2020)
- [8] Chalasani, P., Wang, L., Roy, R., Simaan, N., Taylor, R.H., Kobilarov, M.: Concurrent nonparametric estimation of organ geometry and tissue stiffness using continuous adaptive palpation. In: 2016 IEEE International Conference on Robotics and Automation (ICRA), pp. 4164–4171 (2016).

IEEE

- [9] Wang, L., Chen, Z., Chalasani, P., Yasin, R.M., Kazanzides, P., Taylor, R.H., Simaan, N.: Force-controlled exploration for updating virtual fixture geometry in model-mediated telemanipulation. *Journal of Mechanisms and Robotics* **9**(2), 021010 (2017)
- [10] Yasin, R., Chalasani, P., Zevallos, N., Shahbazi, M., Li, Z., Deguet, A., Kazanzides, P., Choset, H., Taylor, R.H., Simaan, N.: Evaluation of hybrid control and palpation assistance for situational awareness in telemanipulated task execution. *IEEE Transactions on Medical Robotics and Bionics* **3**(1), 31–43 (2020)
- [11] Taylor, R.H., Mittelstadt, B.D., Paul, H.A., Hanson, W., Kazanzides, P., Zuhars, J.F., Williamson, B., Musits, B.L., Glassman, E., Bargar, W.L.: An image-directed robotic system for precise orthopaedic surgery. *IEEE Transactions on Robotics and Automation* **10**(3), 261–275 (1994)
- [12] Kazanzides, P.: Robot assisted surgery: The robodoc® experience. In: *INTERNATIONAL SYMPOSIUM ON ROBOTICS* (1999)
- [13] Chalasani, P., Wang, L., Yasin, R., Simaan, N., Taylor, R.H.: Preliminary evaluation of an online estimation method for organ geometry and tissue stiffness. *IEEE Robotics and Automation Letters* **3**(3), 1816–1823 (2018)
- [14] Yasin, R., Chalasani, P., Zevallos, N., Shahbazi, M., Li, Z., Deguet, A., Kazanzides, P., Choset, H., Taylor, R.H., Simaan, N.: Evaluation of hybrid control and palpation assistance for situational awareness in telemanipulated task execution. *TMRB* (2021)
- [15] Shi, Y., Deng, X., Tong, Y., Li, R., Zhang, Y., Ren, L., Si, W.: Synergistic digital twin and holographic augmented-reality-guided percutaneous puncture of respiratory liver tumor. *IEEE Transactions on Human-Machine Systems* **52**(6), 1364–1374 (2022)
- [16] Laaki, H., Miche, Y., Tammi, K.: Prototyping a digital twin for real time remote control over mobile networks: Application of remote surgery. *Ieee Access* **7**, 20325–20336 (2019)
- [17] Bonne, S., Panitch, W., Dharmarajan, K., Srinivas, K., Kincade, J.-L., Low, T., Knoth, B., Cowan, C., Fer, D., Thananjeyan, B., *et al.*: A digital twin framework for telesurgery in the presence of varying network quality of service. In: *2022 IEEE 18th International Conference on Automation Science and Engineering (CASE)*, pp. 1325–1332 (2022). IEEE
- [18] Lungu, A.J., Swinkels, W., Claesen, L., Tu, P., Egger, J., Chen, X.: A review on the applications of virtual reality, augmented reality and mixed

- reality in surgical simulation: an extension to different kinds of surgery. *Expert review of medical devices* **18**(1), 47–62 (2021)
- [19] Aguilar-Salinas, P., Gutierrez-Aguirre, S.F., Avila, M.J., Nakaji, P.: Current status of augmented reality in cerebrovascular surgery: a systematic review. *Neurosurgical Review* **45**(3), 1951–1964 (2022)
- [20] Kockro, R.A., Tsai, Y.T., Ng, I., Hwang, P., Zhu, C., Agusanto, K., Hong, L.X., Serra, L.: Dex-ray: augmented reality neurosurgical navigation with a handheld video probe. *Neurosurgery* **65**(4), 795–808 (2009)
- [21] Agha, R.A., Fowler, A.J.: The role and validity of surgical simulation. *International surgery* **100**(2), 350–357 (2015)
- [22] Munawar, A., Li, Z., Kunjam, P., Nagururu, N., Ding, A.S., Kazanzides, P., Looi, T., Creighton, F.X., Taylor, R.H., Unberath, M.: Virtual reality for synergistic surgical training and data generation. *Computer Methods in Biomechanics and Biomedical Engineering: Imaging & Visualization* **10**(4), 366–374 (2022)
- [23] Munawar, A., Li, Z., Nagururu, N., Trakimas, D., Kazanzides, P., Taylor, R.H., Creighton, F.X.: Fully immersive virtual reality for skull-base surgery: Surgical training and beyond. *arXiv preprint arXiv:2302.13878* (2023)
- [24] Razavi, C.R., Wilkening, P.R., Yin, R., Barber, S.R., Taylor, R.H., Carey, J.P., Creighton, F.X.: Image-guided mastoidectomy with a cooperatively controlled end micro-surgery robot. *Otolaryngology–Head and Neck Surgery* **161**(5), 852–855 (2019)
- [25] Yaniv, Z.: Which pivot calibration? In: *Medical Imaging 2015: Image-guided Procedures, Robotic Interventions, and Modeling*, vol. 9415, pp. 542–550 (2015). SPIE
- [26] Kabsch, W.: A solution for the best rotation to relate two sets of vectors. *Acta Crystallographica Section A: Crystal Physics, Diffraction, Theoretical and General Crystallography* **32**(5), 922–923 (1976)
- [27] Feng, L., Wilkening, P., Sevimli, Y., Balicki, M., Olds, K.C., Taylor, R.H.: Accuracy assessment and kinematic calibration of the robotic endoscopic microsurgical system. In: *2016 38th EMBC*, pp. 5091–5094 (2016). IEEE
- [28] Schenker, P.S.: Sensor fusion iv: Control paradigms and data structures; proceedings of the meeting, boston, ma, nov. 12-15, 1991. Technical report, Society of Photo-Optical Instrumentation Engineers (SPIE Proceedings. Vol. 1611) (1992)

- [29] Zhang, Z.: A flexible new technique for camera calibration. *IEEE Transactions on pattern analysis and machine intelligence* **22**(11), 1330–1334 (2000)
- [30] Horaud, R., Dornaika, F.: Hand-eye calibration. *The international journal of robotics research* **14**(3), 195–210 (1995)
- [31] Furrer, F., Fehr, M., Novkovic, T., Sommer, H., Gilitschenski, I., Siegart, R.: Evaluation of combined time-offset estimation and hand-eye calibration on robotic datasets. In: *Field and Service Robotics: Results of the 11th International Conference*, pp. 145–159 (2018). Springer
- [32] Holland, M.T., Mansfield, K., Mitchell, A., Burchiel, K.J.: Hidden error in optical stereotactic navigation systems and strategy to maximize accuracy. *Stereotactic and Functional Neurosurgery* **99**(5), 369–376 (2021)
- [33] Kennedy KL, L.J.: Mastoidectomy. <https://www.ncbi.nlm.nih.gov/books/NBK559153/> Accessed 2023-2-5
- [34] Milletari, F., Navab, N., Ahmadi, S.-A.: V-Net: Fully Convolutional Neural Networks for Volumetric Medical Image Segmentation. In: *2016 Fourth International Conference on 3D Vision (3DV)*, pp. 565–571 (2016)
- [35] Li, Z., Shu, H., Liang, R., Goodridge, A., Sahu, M., Creighton, F.X., Taylor, R.H., Unberath, M.: Tatio: Vision-based joint tracking of anatomy and tool for skull-base surgery. *arXiv preprint arXiv:2212.14131* (2022)
- [36] Li, Z., Liu, X., Drenkow, N., Ding, A., Creighton, F.X., Taylor, R.H., Unberath, M.: Revisiting stereo depth estimation from a sequence-to-sequence perspective with transformers. In: *Proceedings of the IEEE/CVF International Conference on Computer Vision*, pp. 6197–6206 (2021)
- [37] Li, Z., Drenkow, N., Ding, H., Ding, A.S., Lu, A., Creighton, F.X., Taylor, R.H., Unberath, M.: On the sins of image synthesis loss for self-supervised depth estimation. *arXiv preprint arXiv:2109.06163* (2021)
- [38] Li, Z., Gordon, A., Looi, T., Drake, J., Forrest, C., Taylor, R.H.: Anatomical mesh-based virtual fixtures for surgical robots. In: *2020 IEEE/RSJ International Conference on Intelligent Robots and Systems (IROS)*, pp. 3267–3273 (2020). IEEE